Journal for Geometry and Graphics
Volume 4 (2000), No. 1, 31–53.

On Piecewise Linear Approximation of Quadratic Functions

Helmut Pottmann[1], **Rimvydas Krasauskas**[2], **Bernd Hamann**[3], **Kenneth Joy**[3], **Wolfgang Seibold**[4]

[1] *Institute of Geometry, Vienna University of Technology*
Wiedner Hauptstr. 8-10/113, A-1040 Wien, Austria
email: pottmann@geometrie.tuwien.ac.at

[2] *Department of Mathematics, Vilnius University*
Naugarduko 24, 2600 Vilnius, Lithuania
email: Rimvydas.Krasauskas@maf.vtu.lt

[3] *Center for Image Processing and Integrated Computing*
Department of Computer Science
University of California, Davis, CA 95616, USA
email hamann(joy)@cs.ucdavis.edu

[4] *Department of Computer Science, University of Otago*
Box 56, Dunedin, New Zealand

Abstract. We study piecewise linear approximation of quadratic functions defined on $\mathbb{R}^n$. Invariance properties and canonical Caley/Klein metrics that help in understanding this problem can be handled in arbitrary dimensions. However, the problem of optimal approximants in the sense that their linear pieces are of maximal size by keeping a given error tolerance, is a difficult one. We present a detailled discussion of the case $n = 2$, where we can partially use results from convex geometry and discrete geometry. The case $n = 3$ is considerably harder, and thus just a few results can be formulated so far.

Key Words: optimal polygon meshes, piecewise linear approximation, data--dependent triangulation, Voronoi tessellation, power diagram, Delone triangulation, convex geometry, discrete geometry, Cayley-Klein geometry

MSC 1994: 65D15, 65D18.

1. Introduction

Computer graphics and scientific visualization algorithms require the approximation of data by linear pieces. In the context of surface rendering, surfaces must be broken down into

ISSN 1433-8157/\$ 2.50

individual triangles; in the context of volume rendering, where one is concerned with the visualization of trivariate data, one must represent the domain of interest by a set of tetrahedra.

The construction of so-called linear spline approximations of bivariate and trivariate data has been an active area of research over the past few decades. Let us mention the work on data dependent triangulations initiated by N. Dyn et al. [11, 12]. Some contributions are using the curvature behaviour of the function graph for deriving data dependent triangulations and data reduction in given triangulations [25, 26, 27, 33]. The visualization community has developed various hierarchical data representations based on triangulations (see, e.g., [1, 6, 8, 13, 16, 18, 19, 25, 28, 29, 34, 36, 38]). These papers discuss multi-level approximations of functions depending on one, two, or three variables. Unfortunately, only some of the methods are based on a well developed mathematical theory. Thus, we go back to the mathematical foundations of the subject of piecewise linear approximation and try to get insight which shall guide our future research in this direction.

So far, very little research has been done concerning the *optimal approximation of bivariate and trivariate polynomials.* In this paper, we are concerned, primarily, with the construction of optimal triangulations for bivariate and trivariate quadratic functions. Often, one is faced with the problem of rendering scattered data points in the plane or in space with associated function values. A direct approach would simply construct a triangulation for all scattered data points and use the implied linear spline representation for subsequent rendering of the data. This, of course, can lead to redundancy in the data approximation in the following sense: Assuming that the function values vary, at least locally, in a nearly linear or quadratic fashion, a triangulation considering all scattered data points uses more data points than required for representation. If one were to construct, prior to any visualization, a set of quadratic least squares polynomials that approximate a particular subset of the given data within some tolerance, one would only have to worry about the construction of an optimal triangulation of these quadratic polynomials such that the resulting total approximation error is not above some overall threshold.

Little work has been done concerning the optimal triangulation or optimal piecewise linear approximation of graph surfaces of quadratic polynomials. In this context, we call a triangulation optimal if the implied linear spline, consisting of individual simplicial spline segments, is based on a minimal number of simplices (triangles and tetrahedra in the bivariate and trivariate cases, respectively). The question we study is the following one: Given the coefficients of a quadratic polynomial and an approximation tolerance, how does one have to triangulate the domain of the polynomial such that the resulting error is below or equal to the tolerance and the number of simplices minimal? Moreover, we do not always restrict to triangulations and consider piecewise linear representations over non-simplicial cells as well. In particular, we study the cases of bivariate and trivariate graph surfaces, which are, at least in the context of visualization, the most important cases.

2. Normal forms and invariance properties

We denote points in $\mathbb{R}^n$ by $\mathbf{x} = (x_1, \dots, x_n)^t$ and consider the quadratic function $f : \mathbb{R}^n \to \mathbb{R}$,

$$f(\mathbf{x}) = \mathbf{x}^t \cdot Q \cdot \mathbf{x} + \mathbf{b}^t \cdot \mathbf{x} + c. \tag{1}$$

Here, Q is a symmetric $n \times n$ matrix and $\mathbf{b}$ is a constant vector in $\mathbb{R}^n$. Our goal is the study of piecewise linear approximants to f. Thus, we need to consider quadratic forms

$$f(\mathbf{x}) = \mathbf{x}^t \cdot Q \cdot \mathbf{x} \tag{2}$$

only since the linear term can be added to the approximant without changing the error.

Concerning the error of an approximant l_f to f over a finite domain $D \subset \mathbb{R}^n$, we use the L^p error,

$$\|f - l_f\|_p = (\text{int}_D |f(\mathbf{x}) - l_f(\mathbf{x})|^p d\mathbf{x})^{\frac{1}{p}}. \tag{3}$$

In particular, we consider the maximum norm (Chebyshev norm; $p = \infty$), which is the maximum absolute value of the difference of the two functions on D. On an infinite domain, which is $\mathbb{R}^n$ in our case, we define the L^p error as maximum L^p error occurring in the linear pieces of the approximant.

Geometrically, it is convenient to study the graph Φ of the function f. This is a quadratic hypersurface in $\mathbb{R}^{n+1}$,

$$\Phi : x_{n+1} = \mathbf{x}^t \cdot Q \cdot \mathbf{x}. \tag{4}$$

A piecewise linear approximant l_f to f has some polytope Λ_f as its graph. Note, however, that the approximation error to Φ is *not* measured in a canonical Euclidean norm in $\mathbb{R}^{n+1}$. It is measured on lines parallel to the x_{n+1}-axis and appropriately integrated depending on the specific norm we are using.

Of fundamental importance for the following considerations are those affine maps $\bar{\alpha}$ in $\mathbb{R}^{n+1}$ which map Φ as a whole onto itself and which do not change the error. In view of the used error norms, $\bar{\alpha}$ maps a line parallel to the x_{n+1}-axis to an x_{n+1}-parallel and it preserves the differences of the x_{n+1}-coordinates on such lines. Because of the last two requirements $\bar{\alpha} : (\mathbf{x}, x_{n+1}) \mapsto (\mathbf{x}', x'_{n+1})$ is of the form

$$\begin{aligned} \mathbf{x}' &= A \cdot \mathbf{x} + \mathbf{b}, \\ x'_{n+1} &= x_{n+1} + \mathbf{c}^t \cdot \mathbf{x} + d. \end{aligned} \tag{5}$$

Hence, it is an extension of an affine map in $\mathbb{R}^n$,

$$\alpha : \ \mathbf{x} \mapsto A \cdot \mathbf{x} + \mathbf{b}, \tag{6}$$

with some regular $n \times n$-matrix A. Since $\bar{\alpha}$ maps Φ onto itself, $x_{n+1} = \mathbf{x}^t \cdot Q \cdot \mathbf{x}$ implies $x'_{n+1} = \mathbf{x}'^t \cdot Q \cdot \mathbf{x}'$ for all $\mathbf{x}$. Inserting the representation for $\bar{\alpha}$, we get the identity

$$\mathbf{x}^t \cdot Q \cdot \mathbf{x} + \mathbf{c}^t \cdot \mathbf{x} + d = (A \cdot \mathbf{x} + \mathbf{b})^t \cdot Q \cdot (A \cdot \mathbf{x} + \mathbf{b}).$$

It is equivalent to

$$A^t \cdot Q \cdot A = Q, \tag{7}$$

and

$$\mathbf{c}^t = 2\mathbf{b}^t \cdot Q \cdot A, \ \ d = \mathbf{b}^t \cdot Q \cdot \mathbf{b}. \tag{8}$$

We call a matrix satisfying equation (7) $Q - orthogonal$. Hence, any of the transformations $\bar{\alpha}$ we are looking for can be obtained in the following way: Choose an affine map α in $\mathbb{R}^n$ to a Q-orthogonal matrix A and an arbitrary translational part $\mathbf{b}$. This defines $\bar{\alpha}$ uniquely via (5) and (8).

Example 2.1. Let $n = 2$ and $f(\mathbf{x}) = x_1^2 + x_2^2$, i.e., Q is the identity matrix. Now, (7) is the condition for an orthogonal matrix A. Hence, α is a Euclidean motion in the plane. The graph surface Φ of f is a paraboloid of revolution. Any Euclidean motion α in the plane can be extended to an affine transformation $\bar{\alpha}$ in $\mathbb{R}^3$, which maps the paraboloid onto itself and preserves distances of points in $\mathbb{R}^3$ to Φ measured in the x_3-direction. A piecewise linear

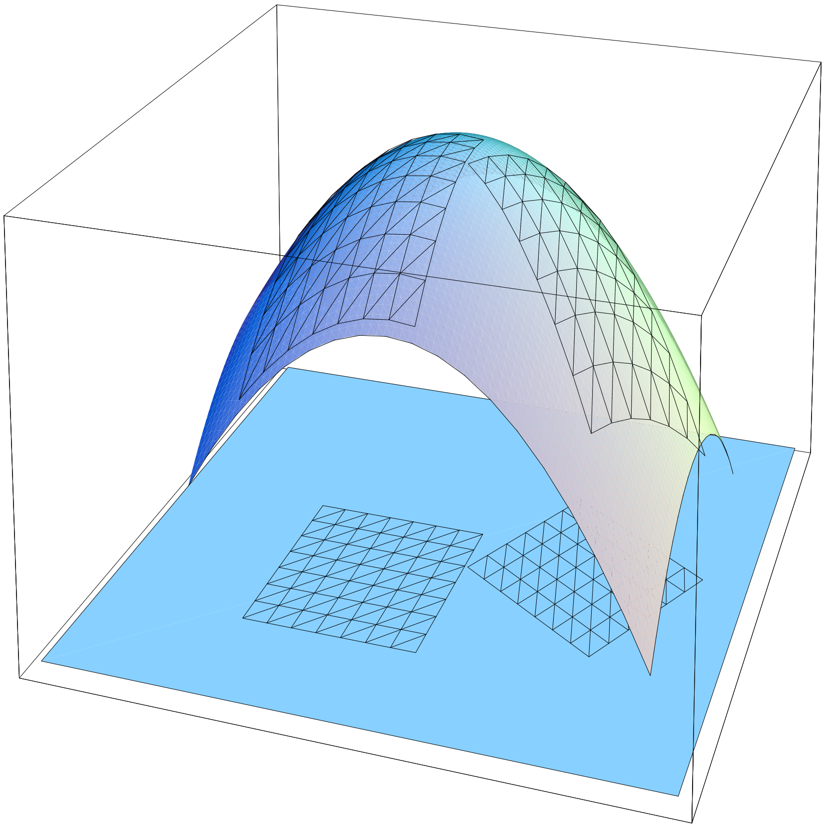

Figure 1: Graphs of two approximants with the same error

approximant l_f has some graph polyhedron Λ_f. Under the map $\bar{\alpha}$, this polyhedron is mapped to another polyhedron Λ'_f. By construction of $\bar{\alpha}$, the two polyhedra belong to *two piecewise linear approximants of f which exhibit the same L^p error* (cf. Figure 1)

Example 2.2. The previous example is easily extended to arbitrary dimension n and an arbitrary definite matrix Q. Since f and $-f$ are equivalent functions for our approximation problem, we may assume that Q is positive definite. Equation (7) tells us that Q is an orthogonal matrix in a Euclidean metric in $\mathbb{R}^n$, which is based on the inner product

$$\langle \mathbf{x}, \mathbf{y} \rangle := \mathbf{x}^t \cdot Q \cdot \mathbf{y}.$$

The corresponding squared Euclidean distance of two points $\mathbf{x}, \mathbf{y}$ is

$$d^2(\mathbf{x}, \mathbf{y}) = \langle \mathbf{x} - \mathbf{y}, \mathbf{x} - \mathbf{y} \rangle = (\mathbf{x} - \mathbf{y})^t \cdot Q \cdot (\mathbf{x} - \mathbf{y}).$$

Clearly, the L^p error-preserving map α is a Euclidean motion (congruence transformation) in this n-dimensional Euclidean geometry. To understand the situation, it is sufficient to apply an affine map which maps the unit sphere (ellipsoid) $\mathbf{x}^t \cdot Q \cdot \mathbf{x} = 1$ of the general case to the standard unit sphere $\mathbf{x}^t \cdot \mathbf{x} = 1$. The previously described general Euclidean metric is mapped to the canonical Euclidean metric in $\mathbb{R}^n$. Maps α, which preserve the L^p error, appear now as standard Euclidean motions in $\mathbb{R}^n$.

Even if Q is not definite, the mappings α are well-studied transformations. They may be viewed as motions (or special similarities in the case of a singular matrix Q) in so-called *affine Cayley-Klein geometries* [17], which are based on the matrix Q. Their extensions $\bar{\alpha}$

to $\mathbb{R}^n$, which we use to transform an approximant, are also certain motions in Cayley-Klein spaces, which are "isotropic" in the x_{n+1}-direction. In the latter geometry, the graph surface Φ of f serves as a sphere and mappings $\bar{\alpha}$ are motions of the sphere into itself. Just like a Euclidean self-motion of the sphere maps a polyhedral approximant of the sphere onto an equally good approximant, mappings $\bar{\alpha}$ do the same with the graph polytopes of piecewise linear approximants to f. For further investigations, we have to distinguish between (i) a regular matrix Q and (ii) a singular matrix Q.

For a regular matrix Q, equation (7) implies $|\det A| = 1$. Let us now apply a mapping $\bar{\alpha}$ to a piecewise linear approximant l_f of f over a domain D in the sense explained above. We get an approximant l'_f over $\alpha(D)$ whose L^p error is the same as the L^p error of l_f. This follows from the fact that $\bar{\alpha}$ preserves differences of function values between the approximant and f (i.e., the integrand in (3)) and via $d\mathbf{x}' = |\det A| d\mathbf{x} = d\mathbf{x}$.

For a singular matrix Q, equation (7) does not imply $|\det A| = 1$, and obviously we have to impose this as an additional condition for getting the invariance property of the L^p-error (except for $p = \infty$, where no integration is necessary). We have proved an extension of results in [32] and [10], summarized in the following theorem:

Theorem 7 sl To any quadratic function $f = \mathbf{x}^t \cdot Q \cdot \mathbf{x}$ in $\mathbb{R}^n$ there exists a group of affine transformations α in $\mathbb{R}^n$, characterized by equations (6) and (7), which may be viewed as congruence transformations in an affine Cayley-Klein space and which possess the following property: Any α may be extended via (5) and (8) to an affine map $\bar{\alpha}$ in $\mathbb{R}^{n+1}$; $\bar{\alpha}$ maps the graph polytope of a piecewise linear approximant l_f of f over a domain $D \subset \mathbb{R}^n$ onto the graph polytope of a piecewise linear approximant l'_f of f, such that the L^p error between f and l'_f over $\alpha(D)$ is the same as the L^P error between f and l_f over D. In case of a singular matrix Q and $p \neq \infty$, an additional condition for the invariance of the L^p error is $|\det A| = 1$.

As outlined in Example 2.2, it is sufficient to view *affine normal forms of* f. An affine map $\mathbf{x} \mapsto \mathbf{x}'$, where $\mathbf{x} = B \cdot \mathbf{x}'$, maps a level set $\mathbf{x}^t \cdot Q \cdot \mathbf{x} = c$ onto the level set $\mathbf{x}'^t \cdot B^t \cdot Q \cdot B \cdot \mathbf{x}' = c$. Since Q is symmetric, all eigenvalues are real, and therefore an orthogonal matrix B exists, such that the matrix $Q' = B^t \cdot Q \cdot B$ is a diagonal matrix; its entries are the eigenvalues of Q. Appending an affine map composed of scaling transformations in the direction of the eigenvectors, we obtain the well-known fact that only the signs of the eigenvalues are important and that B can be chosen such that the diagonal elements in Q' are $1, -1$ or 0. Treating f and $-f$ equivalently, there are three normal forms for $n = 2$ (with diagonals $(1,1), (1,-1), (1,0)$) and five cases for $n = 3$ (with diagonals $(1,1,1), (1,1,-1), (1,1,0), (1,-1,0), (1,0,0)$). In sections 4 and 5, we present a detailed discussion of these types in two and three dimensions.

3. Maximum errors on k-dimensional faces

In this section, we study the L^∞ error and at first consider only those piecewise linear approximations l_f where interpolation occurs at the vertices of the graph polytope. In other words, the vertices of the graph polytope Λ_f lie on the graph hypersurface Φ of f.

At first we determine the maximum error along an *edge* $\mathbf{v}_i\mathbf{v}_j$ in $\mathbb{R}^n$. With $f(\mathbf{v}_i) = l_f(\mathbf{v}_i), f(\mathbf{v}_j) = l_f(\mathbf{v}_j)$ and an elementary property of a univariate quadratic function, the maximum error ϵ occurs at the midpoint $(\mathbf{v}_i + \mathbf{v}_j)/2$. Its value is

$$\epsilon = \left| \frac{f(\mathbf{v}_i) + f(\mathbf{v}_j)}{2} - f\left(\frac{\mathbf{v}_i + \mathbf{v}_j}{2}\right) \right| = \frac{1}{4} \left| (\mathbf{v}_i - \mathbf{v}_j)^t \cdot Q \cdot (\mathbf{v}_i - \mathbf{v}_j) \right|. \tag{9}$$

The squared distance of the two vertices $\mathbf{v}_i, \mathbf{v}_j$ in the Caley-Klein metric induced by Q (or f) is defined by

$$d^2(\mathbf{v}_i, \mathbf{v}_j) = (\mathbf{v}_i - \mathbf{v}_j)^t \cdot Q \cdot (\mathbf{v}_i - \mathbf{v}_j). \tag{10}$$

For a definite matrix Q, we can restrict the discussion to a positive definite matrix Q, and then d is real. In the indefinite case, we have a quadratic cone of isotropic vectors $\mathbf{i}$ with $d(\mathbf{i}, \mathbf{i}) = 0$. It separates the directions on which the distance measurement yields real results from those where we have imaginary distances. Of course, the squared distance is always real and its absolute value determines the error. We can summarize this by the following lemma:

Lemma 2 sl On a straight line segment $\mathbf{v}_i\mathbf{v}_j$, the maximum error between a linear function l_f and a quadratic function f with $f(\mathbf{v}_i) - l_f(\mathbf{v}_i) = f(\mathbf{v}_j) - l_f(\mathbf{v}_j) = 0$ occurs at the midpoint and it equals one fourth of the absolute value of the squared distance of the two points $\mathbf{v}_i, \mathbf{v}_j$ in the Cayley-Klein metric induced by f.

Next, we consider a definite function f. It induces a Euclidean metric in $\mathbb{R}^n$ (Example 2.2). Let

$$l_f(\mathbf{x}) = \mathbf{c}^t \cdot \mathbf{x} + d$$

be a linear function. The gradient of the difference function $e = l_f - f$ is

$$\nabla e = 2Q \cdot \mathbf{x} - \mathbf{c}.$$

It vanishes at the point

$$\mathbf{m} = \frac{1}{2} Q^{-1} \cdot \mathbf{c}. \tag{11}$$

The definite matrix $2Q$ is the Hessian of e, and therefore a local extremum of e occurs at $\mathbf{m}$. Let us consider the graphs in $\mathbb{R}^{n+1}$. The graph hyperplane Λ_f of l_f is $x_{n+1} = \mathbf{c}^t \cdot \mathbf{x} + d$. The graph paraboloid Φ of f, which is $x_{n+1} = \mathbf{x}^t \cdot Q \cdot \mathbf{x}$, has a tangent hyperplane at $(\mathbf{m}, f(\mathbf{m}))$, which is parallel to Λ_f. The not necessarily real intersection $\Lambda_f \cap \Phi$ is a quadratic surface; its projection Σ_0 into $\mathbb{R}^n$ is the set of points with error $e = 0$,

$$\Sigma_0 : \ \mathbf{x}^t \cdot Q \cdot \mathbf{x} = \mathbf{c}^t \cdot \mathbf{x} + d. \tag{12}$$

The midpoint form is

$$(\mathbf{x} - \mathbf{m})^t \cdot Q \cdot (\mathbf{x} - \mathbf{m}) = d + \mathbf{m}^t \cdot Q \cdot \mathbf{m}. \tag{13}$$

Assuming that Σ_0 is real, the right hand side is positive,

$$d + \mathbf{m}^t \cdot Q \cdot \mathbf{m} = \rho^2.$$

The set of points with error $e = 0$ is a *sphere* Σ_0 *with radius* ρ *and center* $\mathbf{m}$ in our Euclidean metric. The error e at an arbitrary point $\mathbf{x}$ can be written as

$$e(\mathbf{x}) = |(\mathbf{x} - \mathbf{m})^t \cdot Q \cdot (\mathbf{x} - \mathbf{m}) - \rho^2| = |d^2(\mathbf{x}, \mathbf{m}) - \rho^2|. \tag{14}$$

(Note: This formula also holds if $\rho^2 \leq 0$.) For $\rho = 0$, Σ_0 has only one real point $\mathbf{m}$; in the complex extension it is an imaginary cone with the real vertex $\mathbf{m}$. Finally, $\rho^2 < 0$ characterizes an imaginary sphere with center $\mathbf{m}$ and imaginary radius $i\sqrt{|\rho^2|}$. In all cases, equation (14) shows that *the error* $e(\mathbf{x})$ *equals the absolute value of the power of* $\mathbf{x}$ *with respect to the sphere* Σ_0*, whose points are characterized by zero error.*

Returning to a piecewise linear approximation l_f of f, we are interested in the tessellation of $\mathbb{R}^n$ whose n-dimensional cells are the domains of the linear pieces of l_f. We pick a cell with vertices $\mathbf{v}_1, \ldots, \mathbf{v}_j$. Assuming interpolation at the vertices, they lie on the real sphere Σ_0. We can now state the following result (Figure 2):

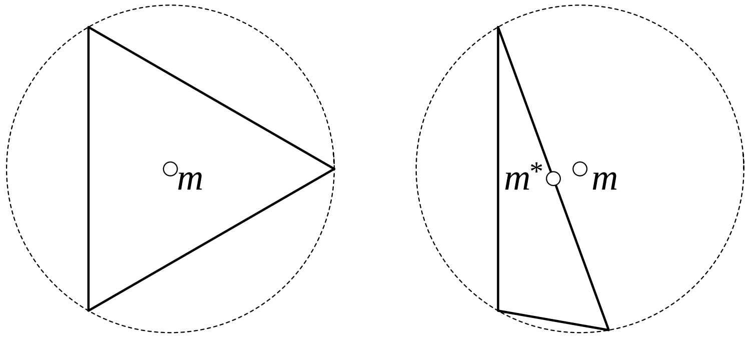

Figure 2: Maximum errors in the definite case

Lemma 3 sl Consider a piecewise linear approximant l_f of a definite quadratic function f on $\mathbb{R}^n$ and let C be an n-dimensional cell of the approximant with interpolating vertices $\mathbf{v}_1, \ldots, \mathbf{v}_j$. These vertices lie on a sphere Σ_0 (with center $\mathbf{m}$ and radius ρ) in the induced Euclidean metric. In case that its center $\mathbf{m}$ is contained in C, the maximum error occurs there, and the error value is the squared radius ρ^2 of Σ_0. Otherwise, the error occurs at the point $\mathbf{m}^*$ on the boundary of C which is closest to $\mathbf{m}$; the error is $e_{max} = |d^2(\mathbf{m}^*, \mathbf{m}) - \rho^2|$ in this case. Denoting the dimension of the face C_k on which $\mathbf{m}^*$ is lying by k, we can interpret $\mathbf{m}^*$ as center of a k-sphere with squared radius e_{max}, which contains all vertices of C_k.

Note that it is sufficient to prove this result for the normal form $f = x_1^2 + \ldots + x_n^2$ and a constant function l_f. This follows from Theorem 7. It is also clear that a similar result holds for k-dimensional faces of the tessellation. Again, the maximum error occurs at the center $\mathbf{m}_k$ of the circumscribed k-sphere of the face or at the point on the boundary which is closest to an outside center. In particular, for $k = 1$ we obtain Lemma 2.

Dual to vertex interpolation we may require that the graph hyperplanes of the n-dimensional cells in the piecewise linear approximation are tangent hyperplanes to the graph paraboloid Φ. We may say that the graph polytope of the approximant is circumscribed to the paraboloid Φ. In this case, all spheres Σ_0^i with error 0 reduce to points $\mathbf{m}^i$ (over $\mathbb{R}$). It is well known that the tessellation formed by the cells in $\mathbb{R}^n$ is the *Voronoi diagram* of the set of points $\mathbf{m}^i$.

More generally, we may drop the tangency condition. Then the n-dimensional cells C_i in $\mathbb{R}^n$ determine a set of spheres Σ_0^i with zero error; clearly, good approximants will not cause imaginary spheres. All points in a cell C_i have smaller power to the sphere Σ_0^i of their cell than to any other sphere Σ_0^j (by equation (14)). It is a cell of the *power diagram* to the set of spheres Σ_i as studied by F. AURENHAMMER [2]. *The tessellation in $\mathbb{R}^n$ determined by a piecewise linear approximant is the power diagram to the set of zero-error spheres of its linear pieces* (Fig. 3). Of course, this diagram has to be constructed in the induced Euclidean metric and we are considering convex graph polytopes, hence convex tiles of the tessellation only.

In the *indefinite case*, formula (14) is still valid. However, since the Hessian $2Q$ of the error function is indefinite, a local extremum never occurs at $\mathbf{m}$. Hence, *the maximum error in an n-dimensional cell must occur on its boundary.* It occurs on a k-dimensional face on which the restriction of f is definite. Hence, we consider the definite case again.

For a *semidefinite matrix* Q, we have to project parallel to the eigenspace of the eigenvalue 0 and then either obtain a definite or indefinite case. Hence, for the determination of the maximum error we eventually treat a definite case. Examples will be given in the following sections.

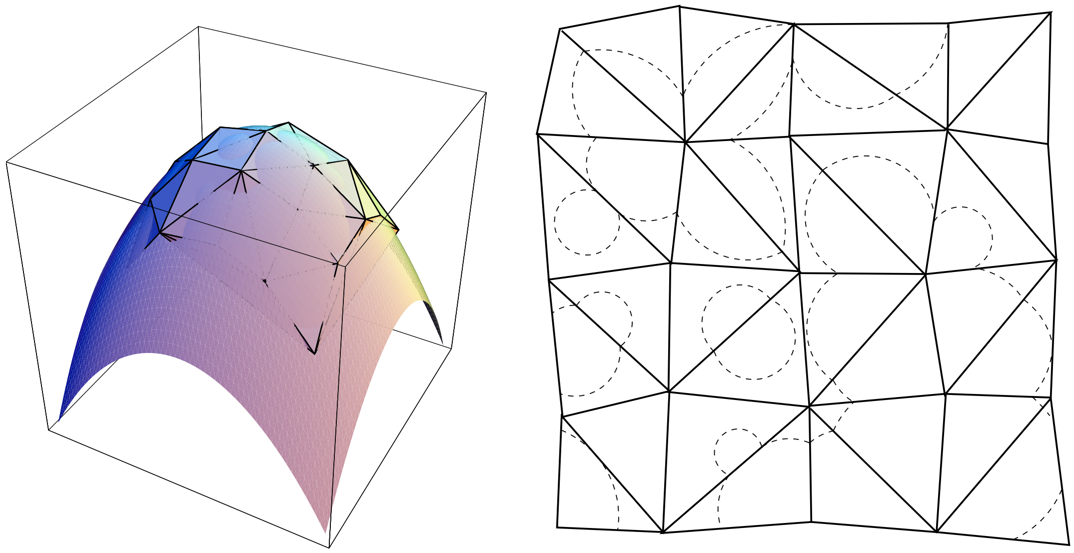

Figure 3: Power diagram in the plane (right) as projection of a convex polyhedron and the intersections of its faces with a paraboloid (left)

4. The definite case and relations to convex and discrete geometry

To handle the definite case, we may assume that f is a positive definite quadratic form. Piecewise linear approximations to f possess an intimate relation to a variety of results from convex geometry and discrete geometry, some of which we review briefly (for a survey on the rich literature, see [23]).

Let us first discuss the case of given vertices $\mathbf{v}_1, \ldots, \mathbf{v}_N$, at which f shall be interpolated. We shall construct a triangulation with vertices $\mathbf{v}_i$ whose associated piecewise linear approximant best approximates f in the L^p sense. Investigating the graphs in $\mathbb{R}^{n+1}$, it is clear that the best approximant has as its graph polytope the lower convex hull of the vertices. As is well known, it corresponds to the *Delaunay triangulation* in the Euclidean metric induced by f. This is a classical result, which has also been treated recently by Melissaratos [32]. Of course, the characterization of the best piecewise linear approximant in $\mathbb{R}^{n+1}$ as lower convex hull of the lifted points is also true for an arbitrary convex function f.

More interesting is the problem of optimal approximants whose knots (i.e., vertices of the polyhedral domains in $\mathbb{R}^n$ on which the linear pieces are defined) are not prescribed. First, we assume that the underlying domain is $\mathbb{R}^n$. We study approximants defined over a tiling of $\mathbb{R}^n$ whose tiles are polytopes and translates of each other.

To describe such tilings, we need a few definitions. Given a basis $B = \{\mathbf{b}_1, \ldots, \mathbf{b}_n\}$ of $\mathbb{R}^n$, all points with integer coordinates in the basis B form a *lattice* $\mathcal{L}$ with basis B. All other bases of $\mathcal{L}$ are related to B by a transformation matrix with integer entries and determinant ± 1. The *determinant* $d(\mathcal{L})$ of $\mathcal{L}$ is the absolute value of the determinant of a basis B. Any translation which maps a lattice point to a lattice point maps the lattice as a whole onto itself. The Voronoi cells [14, 23] in any given Euclidean metric are so-called parallelohedra. They are translates of each other and form a tiling of $\mathbb{R}^n$ (Figure 4). Their volume is $d(\mathcal{L})$. Among these *lattice tilings* we are interested in those which best approximate f. There are at least two reasons for choosing these tilings: A lattice is easy to set up and efficient algorithms exist for computing Voronoi diagrams [14]. Moreover, it is conjectured that optimal solutions belong to lattice tilings anyway.

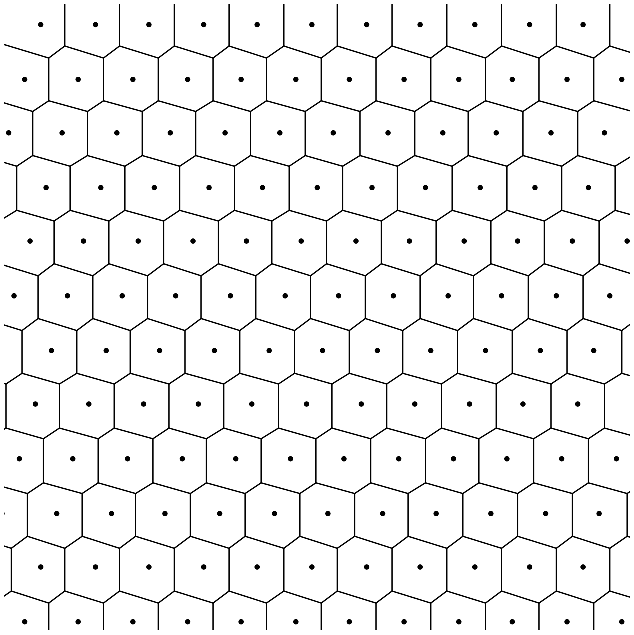

Figure 4: Lattice tiling in the plane

We first study the *maximum norm* and fix the allowed error. Moreover, we assume that the vertices of the cells are interpolating f. Let us pick a cell. It is centrally symmetric with respect to its unique interior lattice point, which we call $\mathbf{m}$. Because of the vertex interpolation property, all vertices of the cell lie on a sphere (with respect to the Euclidean metric induced by f) with center $\mathbf{m}$. According to Lemma 3, the maximum error occurs at $\mathbf{m}$ and equals the squared radius of the sphere. By the invariance property and the translational invariance of the lattice tiling, it is clear that the same error results in every tile. The hyperplanar faces of adjacent tiles carry the intersection of congruent spheres around their centers. Hence, the tiles are the Voronoi cells of the lattice $\mathcal{L}$ with respect to the metric induced by f. An optimal approximation is defined as one whose tiles have maximal volume. The problem is the following: *find the lattice(s) whose Voronoi cells have a circumsphere of a given radius and possess maximum volume.* We will discuss the cases $n = 2$ and $n = 3$ later.

Let us now drop the interpolation condition at the vertices and prescribe the maximum error ϵ. We consider the linear function over a cell. Given this linear function, it is clear from equation (14) that the error is reduced if we perform a translation such that the center $\mathbf{m}$ of the cell agrees with the center of the sphere Σ_0 with error 0. The maximum error inside Σ_0 occurs at $\mathbf{m}$ and equals the squared radius $\epsilon = \rho^2$ of Σ_0. The same error is obtained the concentric sphere with radius $\rho\sqrt{2} = \sqrt{2\epsilon}$. Hence, the largest cell that does not exceed the given error ϵ must be contained in a sphere of radius $\sqrt{2\epsilon}$. Defining the optimal approximant via the largest volume of a cell, we must solve the following problem: *determine the lattice(s) whose Voronoi cells have a given diameter and possess maximum volume.* As a result of the invariance properties, it should be sufficient to take the Voronoi diagram with respect to the induced metric. The solutions for dimensions $n = 2$ and $n = 3$ will be described in the following sections.

In the previous approximation problems one can take a somewhat different point of view, which eventually leads to an equivalent result: One can fix $d(\mathcal{L})$, i.e., the volume of the Voronoi cell, and determine those *lattices whose Voronoi cells have minimum diameter.*

It is conjectured that the solutions to both problems, whether we assume vertex interpolation or not, are the same tilings. Given a tiling and a piecewise linear approximant with vertex interpolation defined over it, the maximum error equals the squared radius ρ^2 of the circumscribed sphere of a tile. Subtraction (addition) of $\rho^2/2$ from (to) the approximating function in case of a positive (negative) definite quadratic form yields an approximant over the same tiling with maximum error $\rho^2/2$. It occurs both at the vertices and the centers of the tiles. Most likely, this is the optimum solution for non-interpolating vertices.

The circumspheres of the tiles form a *lattice covering of* $\mathbb{R}^n$ *with congruent balls*. It is conjectured that the optimal solutions to our problems (even for the L^p error) are the *lattice coverings with smallest covering density* in the discrete geometry sense [23].

A variety of results from approximation of convex bodies can be applied, mainly in case of the L^1 norm and for dimension $n = 2$ [7, 20, 21, 22, 23]. Some of these will be presented in the next section. Here, we just outline the relation to the so-called *moment problem* ([23], pp. 755): let $\omega : [0, +\infty) \mapsto [0, +\infty)$ be a continuous non-decreasing function with $\omega(0) = 0$. Determine those lattices $\mathcal{L}$ with $d(\mathcal{L}) = 1$ for which

$$I = \mathrm{int}\,_V \omega(\|\mathbf{x} - \mathbf{m}\|) d\mathbf{x} \tag{15}$$

is minimal; here, V is a Voronoi cell of the lattice and $\mathbf{m}$ is its center. If we have a circumscribed graph polytope, $I^{\frac{1}{p}}$ with $\omega(t) = t^{2p}$ gives exactly the L^p error over a Voronoi cell V. Therefore, the solution of the moment problem yields lattice tilings over which we can define optimal circumscribed polytopes in the L^p norm.

5. Bivariate functions

5.1. Definite type

For the quadratic function under consideration, we only have to consider $f(\mathbf{x}) = x_1^2 + x_2^2$. Then, the induced metric in $\mathbb{R}^2$ is the canonical Euclidean metric. Geometrically, this means that in the normalized case the graph of the quadratic function is a paraboloid of revolution Φ.

However, everything we do is transformed to the arbitrary definite case by considering the induced Euclidean metric instead of the canonical one. The general case, where Φ is an elliptic paraboloid, is obtained from the normal case by performing an affine map in $\mathbb{R}^2$ and keeping function values at corresponding points. Of course, this is also an affine map between the graphs in $\mathbb{R}^3$, where x_3-coordinates remain unchanged.

Let us first consider the problem of *optimal* L^∞ *triangulations with free knots*. From the previous section we know that by fixing the error ϵ, the triangle has to lie in a circle with radius $\sqrt{2\epsilon}$ without vertex interpolation or in a circle of radius $\sqrt{\epsilon}$ in case of vertex interpolation. It is well known that among all triangles with a given circumcircle the regular triangles have the largest area. Hence, regular triangulations are optimal. From a momentum lemma for power diagrams in [7] it follows that the same result holds for the L^1-error.

Theorem 8 sl Consider a bivariate quadratic function f, whose quadratic form is definite. Then, a L^1 or L^∞ optimal piecewise linear approximant of f over a triangulation of $\mathbb{R}^2$ is defined over a triangulation, which is regular in the Euclidean metric induced by f.

Supported by computational tests, we conjecture that this result also holds for the L^p error. However, the proofs are getting quite involved and thus we confine ourselves to the remaining practically important case $p = 2$. Moreover, we assume vertex interpolation, i.e. an inscribed graph polyhedron.

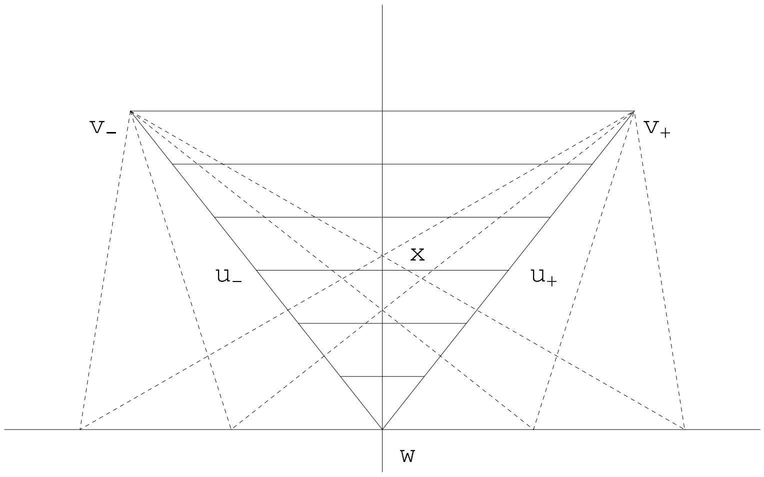

Figure 5:

Theorem 9 sl Let f be a bivariate quadratic function, whose quadratic form is definite, and let us consider piecewise linear approximants over triangulations of $\mathbb{R}^2$ with vertex interpolation. Then, the optimal approximants in the L^2 norm are defined over a triangulation, which is regular in the Euclidean metric induced by f.

Proof: Consider all triangles in $\mathbb{R}^2$ which share an edge and the 'height' over it. These have equal area and we will show below that the L^p error is minimal for the symmetric triangle (third point on the bisector of the vertices of the given edge). This will mean that symmetrizing with respect to the bisector of two vertices reduces the error. The only case, where we can no longer improve is that of a regular triangle.

Let two fixed vertices of the triangle have coordinates $\mathbf{v}_\pm = (\pm a, b)$ and the third $\mathbf{w} = (t, 0)$ is running along x_1-axis. We need to calculate the integral (3) over all such triangles and to show that it has a global minimum when $t = 0$. It is sufficient to prove this for the same integral over every slice parallel to the fixed edge, i.e., over the line segment with endpoints $\mathbf{u}_\pm = \lambda \mathbf{v}_\pm + \mu \mathbf{w}$, $\lambda + \mu = 1$, $\lambda, \mu > 0$ (see Figure 5). Let $\mathbf{x}$ be on the interval $\mathbf{u}_-\mathbf{u}_+$ then $\mathbf{x} = (x, \lambda b)$, where $\mu t - \lambda a \le x \le \mu t + \lambda a$. Hence $f(\mathbf{x}) = x^2 + \lambda^2 b^2$. On the other hand if l_f is a linear interpolant of f in vertices of the triangle then it can be easily evaluated on the endpoints $\mathbf{u}_\pm$:

$$l_f(\mathbf{u}_\pm) = \lambda l_f(\mathbf{v}_\pm) + \mu l_f(\mathbf{w}) = \lambda f(\mathbf{v}_\pm) + \mu f(\mathbf{w}) = \lambda(a^2 + b^2) + \mu t^2.$$

Therefore, l_f is constant (for fixed t) on the interval $\mathbf{u}_-\mathbf{u}_+$. The error in every point is $\ell_f(\mathbf{x}) - f(\mathbf{x}) = \mu t^2 + \lambda(a^2 + b^2) - (x^2 + \lambda^2 b^2) = \mu t^2 - x^2 + c$, where the constant c can be estimated as

$$c = \lambda(a^2 + b^2) - \lambda^2 b^2 > \lambda a^2. \tag{16}$$

In order to simplify the integral

$$I_p(t) = \left(\mathrm{int}_{\,\mathbf{u}_-\mathbf{u}_+} |f(\mathbf{x}) - l_f(\mathbf{x})|^p d\mathbf{x}\right)^{1/p} = \left(\mathrm{int}_{\,\mu t - \lambda a}^{\,\mu t + \lambda a} (\mu t^2 - x^2 + c)^p dx\right)^{1/p},$$

we substitute $t = T/\mu$, $a = A/\lambda$ and $\mu = 1/(M+1)$ (note that $A, M > 0$). In the case $p = 1$ calculations are easy,

$$I_1(T) = \mathrm{int}_{\,T-A}^{\,T+A} \left((M+1)T^2 - x^2 + c\right) dx = 2AMT^2 - \frac{2}{3}A^3 + 2Ac.$$

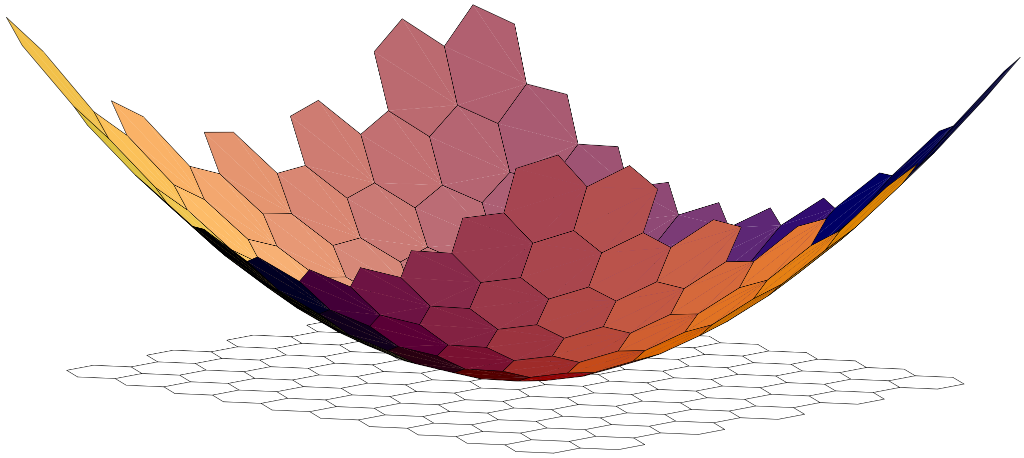

Figure 6: Approximation of a definite quadratic function over a regular hexagonal tiling in the induced Euclidean metric

Since $2AM > 0$, $I_1(T)$ has the unique minimum in $T = 0$, i.e. when $t = 0$. The case $p = 2$ is more complicated. Here it is enough to prove that the square of I_2 has the same minimum:

$$\begin{aligned} I_2^2(T) &= \operatorname{int}_{T-A}^{T+A} \left((M+1)T^2 - x^2 + c\right)^2 dx \\ &= 2AM^2T^4 + \left[\frac{8}{3}A^3 - \frac{4}{3}A^3M + 4AMc\right] T^2 + K\,. \end{aligned}$$

Here K is some constant term which is irrelevant. Since T^4 has a positive coefficient $2AM^2$, it remains to prove that the coefficient in square brackets is non-negative. Expressing the inequality (16) via A and μ

$$c > \lambda a^2 = \frac{1}{\lambda}A^2 = \frac{1}{1-\mu}A^2$$

and applying the backward substitution $M = 1/\mu - 1$ one gets

$$\frac{8}{3}A^3 - \frac{4}{3}A^3M + 4AMc > 4A^3 + \frac{8}{3\mu} > 0.$$

□

For a lattice in the plane, the Voronoi cell is either a parallelogram or a centrally symmetric hexagon. Again, elementary considerations easily lead to the result that, when fixing the diameter of such a figure, the largest area occurs for a regular hexagon. Hence, L^∞-optimal lattice tilings are regular hexagonal tilings (Figure 6). Again, we conjecture that this result holds for any L^p norm. In fact, even the restriction of a lattice tiling seems to be unnecessary, which is obvious for $p = \infty$. Let us present the cases, where proofs are available.

Theorem 10 sl The L^1- or L^∞-optimal piecewise linear approximant on $\mathbb{R}^2$ to a quadratic bivariate function f, whose quadratic form is definite, is defined over a hexagonal tiling of $\mathbb{R}^2$, which is regular in the Euclidean metric induced by f.

Proof: The proof for $p = 1$ follows from the momentum lemma for power diagrams in a recent paper by Böröczky and Ludwig [7]. □

As we have seen in the previous section, the moment problem refers exactly to the case of a circumscribed graph polyhedron. L. Fejes Tóth [15] proved that the minimum of the integral (15) extended over k-gons P with given area is attained for the regular k-gon. We may therefore formulate the following result at hand of the graph surface.

Theorem 11 sl The L^p optimal approximant of an elliptic paraboloid $z = f(x, y)$ by a circumscribed polyhedron with triangular faces is defined over a triangulation in the plane $z = 0$, which is regular in the induced Euclidean metric. Omitting the restriction to triangular faces, the L^p optimal circumscribed polyhedron has hexagonal faces. It is defined over a hexagonal tiling of $\mathbb{R}^2$, which is regular in the Euclidean metric induced by f.

Finally, let us point out that for vertex interpolation and the L^1 error, the optimality of the regular hexagonal tiling has been proved by P.M. GRUBER [20].

5.2. Indefinite type

If the quadratic form f is indefinite, we only have to consider

$$f(\mathbf{x}) = x_1^2 - x_2^2.$$

The graph surface $x_3 = x_1^2 - x_2^2$ is a (right) hyperbolic paraboloid. This case has been addressed by DESNOGUÈS and DEVILLERS [10]. They discuss locally optimal triangulations with given vertices. Among the invariance properties, only the invariance under translations in $\mathbb{R}^2$ has been investigated, for which a proof using symbolic computation is provided. Our invariance results in the second section are more general: The metric induced in $\mathbb{R}^2$ is now a *pseudo-Euclidean* or *Minkowski metric.* Any pseudo-Euclidean (pE) congruence transformation (6) in $\mathbb{R}^2$, belonging to a pE orthogonal matrix A, where

$$A^t \cdot Q \cdot A = Q, \quad Q = \begin{pmatrix} 1 & 0 \\ 0 & 1 \end{pmatrix}, \tag{17}$$

maps a tessellation to a piecewise linear approximant onto a tessellation over which we obtain an equally good approximant in the L^p norm. Transformations with $\det(A) = 1$ belong to pE motions. Here, A is a matrix describing a pE rotation by a pE angle t,

$$A = \begin{pmatrix} \cosh t & \sinh t \\ \sinh t & \cosh t \end{pmatrix}. \tag{18}$$

Let us mention that pE geometry is closely related to Laguerre circle/sphere geometry and to special relativity [4]. Recently, we could also find interesting applications in CAGD [35].

In the following, it is somewhat more convenient to use as normal form of an indefinite quadratic form the representation

$$f(\mathbf{x}) = x_1 x_2.$$

As a result of equation (9), the maximum error over an edge with vertices $\mathbf{a} = (a_1, a_2)$ and $\mathbf{b} = (b_1, b_2)$ is

$$\epsilon = \frac{1}{4} \left| (a_1 - b_1)(a_2 - b_2) \right|. \tag{19}$$

This is a quarter of the area of a rectangle with diagonal **ab** and with edges parallel to the coordinate axes. The lines parallel to the coordinate axes are the projections of the rulings of the hyperbolic paraboloid into $\mathbb{R}^2$. Of course, along these lines the error is 0; they are called the isotropic lines in the pE metric. Thus, neglecting the unimportant factor 1/4, *the error along an edge* **ab** *is the area of the isotropic rectangle with diagonal* **ab** (Figure 7). The

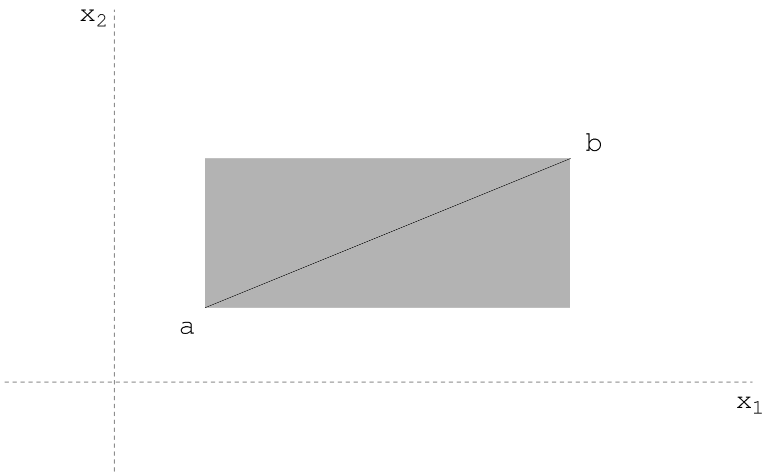

Figure 7: Error along an edge in the indefinite case

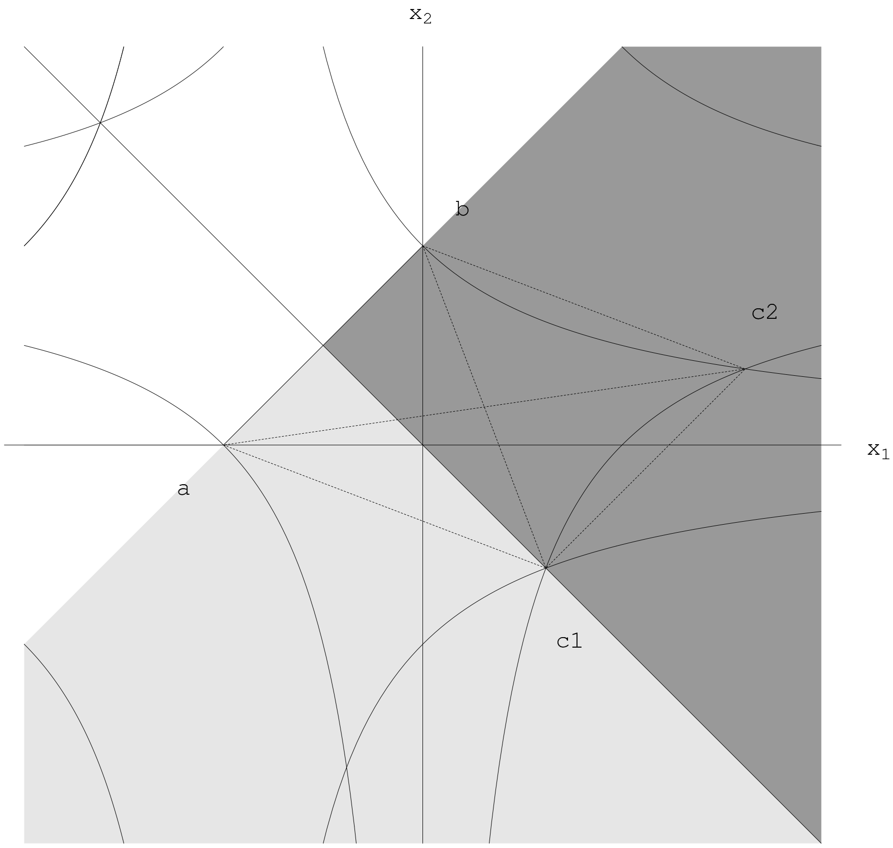

Figure 8: Construction of an optimal triangle in the indefinite case

importance of the error along an edge is based on our earlier observation that, in the indefinite case, the maximum error on a face always occurs at its boundary.

Let us now prescribe the L^∞ error tolerance ϵ and construct optimal triangulations. Of course, this amounts to determining the triangle with largest area and error ϵ. At least one of its edges, say **ab**, must have error ϵ. By a pE motion we can achieve the following special position for its vertices: $\mathsf{a} = (-a, 0)$ and $\mathsf{b} = (0, a), a > 0$. According to equation (19), we have

$$4\epsilon = a^2.$$

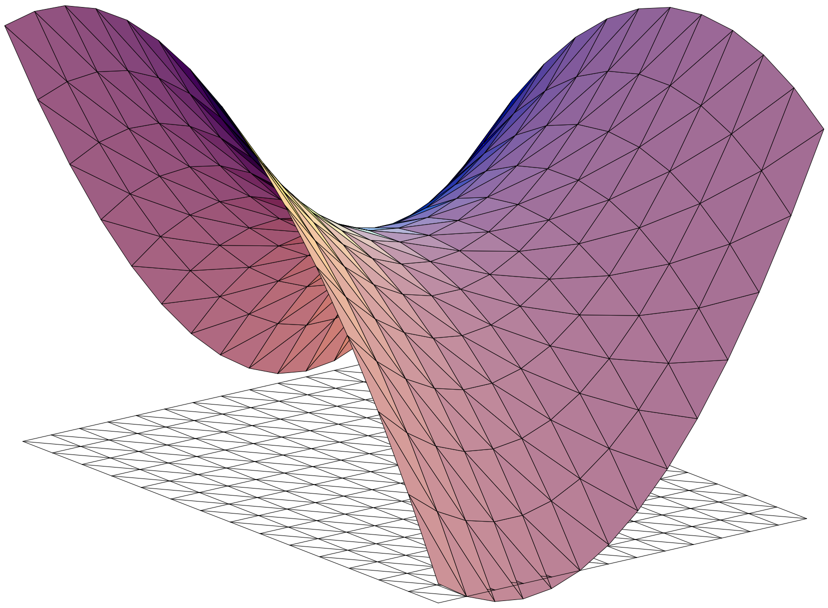

Figure 9: Approximant of a hyperbolic paraboloid defined over a regular pE triangulation

Because of the special position, the pE reflection with respect to the line given by $\mathbf{ab}$ is identical with the Euclidean reflection. Thus, we may assume that the third vertex $\mathbf{c} = (c_1, c_2)$ of the optimal triangle lies in the lower halfplane of the line given by $\mathbf{ab}$, i.e., $c_2 - c_1 - a < 0$. Moreover, the symmetry with respect to the Euclidean bisector $x_1 + x_2 = 0$ of $\mathbf{a}$ and $\mathbf{b}$ is also a pE congruence transformation; thus, we may restrict our search to this symmetry axis and its upper side, $c_1 + c_2 \geq 0$. Since the error on $\mathbf{ac}$ has to be $\leq \epsilon$ (and analogously for $\mathbf{bc}$), $\mathbf{c}$ must lie in the intersection of the domains

$$|(a + c_1)c_2| \leq a^2, \ |c_1(c_2 - a)| \leq a^2,$$

see Figure 8). The domains are bounded by hyperbolae with isotropic asymptotes; in pE geometry they are called "pE circles". Under the outlined constraints, there are two solutions for $\mathbf{c}$ such that all edges of the triangle have the same error

$$\mathbf{c}_1 = \left(a\frac{\sqrt{5}-1}{2}, a\frac{1-\sqrt{5}}{2} \right), \ \mathbf{c}_2 = \left(a\frac{\sqrt{5}+1}{2}, a\frac{3-\sqrt{5}}{2} \right). \tag{20}$$

These triangles may be called *regular* in the pE plane. First, we note that $\mathbf{a}, \mathbf{c}_1, \mathbf{c}_2, \mathbf{b}$ form a parallelogram whose edges and diagonals all have the same error. Both solution triangles have equal area. Any such triangle and its image under reflection at an edge midpoint form a parallelogram and thus a tiling of the plane consisting of optimal triangles only (Figure 9). Hence, we have proved the following result:

Theorem 12 sl An L^∞-optimal piecewise linear approximant over a triangulation of $\mathbb{R}^2$ to a quadratic bivariate function f whose quadratic form is indefinite is defined over a triangulation which is regular in the pseudo-Euclidean metric induced by f. Here, we assume that the linear approximant interpolates the function values at the vertices of the triangulation.

It remains an open question whether these triangulations also yield optimal L^p approximations. Moreover, the idea of giving up vertex interpolation, adding some constant and thereby

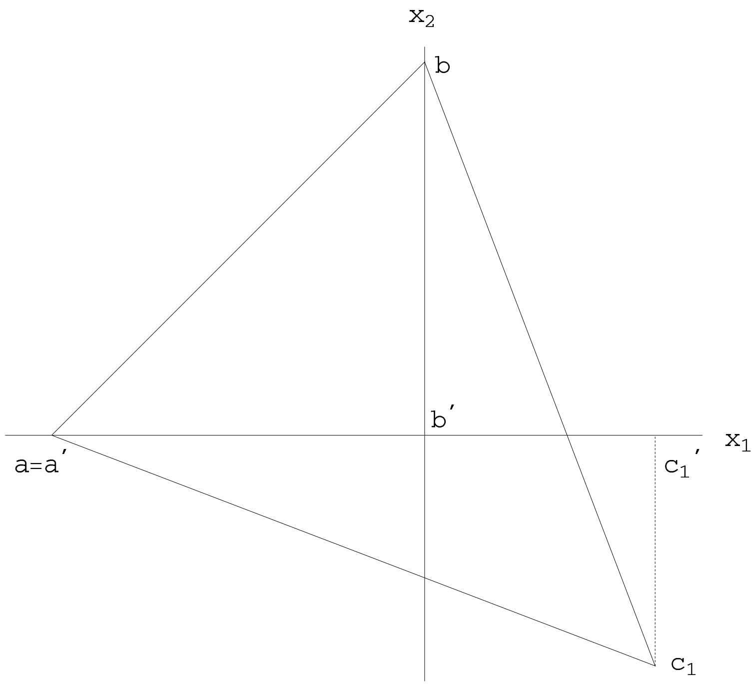

Figure 10: Golden section in pE regular triangles

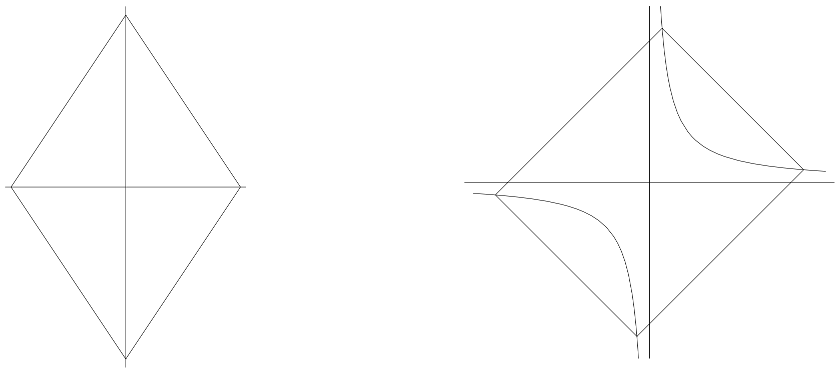

Figure 11: The two cases for quadrilaterals

reducing the L^∞ error by one half does not work since we have both signs for second-order directional derivatives occur. In fact, we conjecture that vertex interpolation is mandatory for any optimal piecewise linear approximant over $\mathbb{R}^2$.

Let us add the following remark on regular triangles in the pE plane: Project vertices $\mathbf{a}, \mathbf{b}, \mathbf{c}_1$ parallel to the x_2-axis, for example, into the x_1-axis (Figure 10). The ratio of distances of these points equals

$$2 : (\sqrt{5} - 1) = (1 + \sqrt{5}) : 2.$$

This ratio is the *golden section* ratio, also called *divine proportion* [5, 31]. Analogously, we can project in the other isotropic direction. Since pE congruence transformations map isotropic lines (parallels to the coordinate axes of our frame) to isotropic lines, we may say: *Projecting the vertices of a regular pE triangle in isotropic direction to a transversal line yields three points which are positioned in the golden section ratio.* Conversely, this property may be used to compute a pE regular triangle.

Analogously, we may study optimal tessellations by *quadrilaterals*. Assuming vertex in-

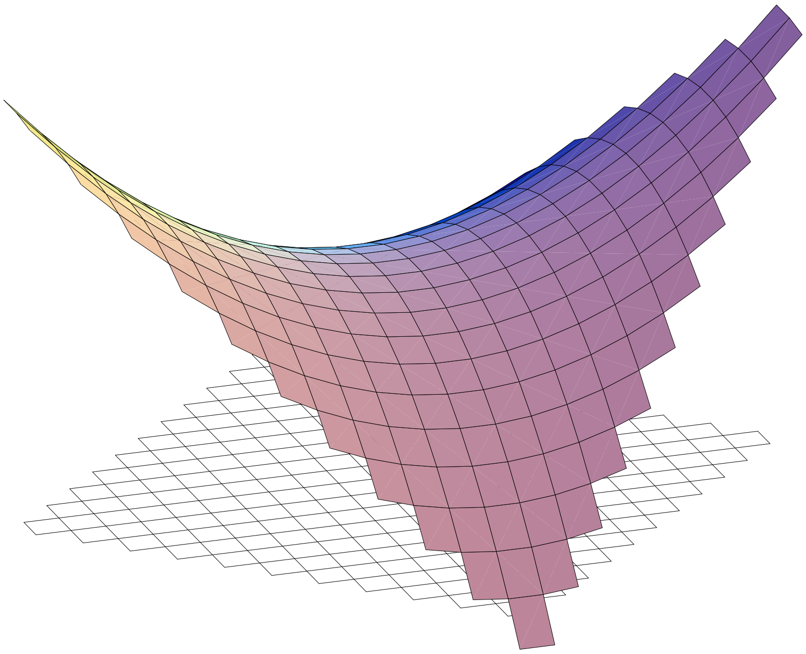

Figure 12: Optimal approximation with quadrilaterals

terpolation, two cases exist (Figure 11). In the first case, the vertices of a quadrilateral lie on a pair of (not parallel) isotropic lines; the graph of the linear function over the quadrilateral is a tangent plane of the hyperbolic paraboloid Φ, spanned by two rulings whose projections are the mentioned isotropic lines. An optimal approximation will have its maximum error on each edge, and it is given by a rhombus whose diagonals are the pair of isotropic lines. Of course, there are infinitely many equally good rhombi with the same diagonals. The resulting tessellation is defined by the diagonal net of a parallelogram grid (Figure 12).

In the second case, the vertices lie on a hyperbola. One can see that the best situation is the one where two points lie on each arc of the hyperbola. However, the area of an approximation with maximum error on each edge is smaller than in the first case. Finally, let us look at n-gons ($n \geq 5$) that are convex and interpolate at the vertices. To obtain convexity all vertices have to be placed on one branch of the hyperbola. This yields a face which is contained in a quarter of a rhombus that defines the same error. Hence, n-gons, $n \geq 5$, do not lead to any improvement. We can state this theorem:

Theorem 13 slConsider L^∞-optimal piecewise linear approximants of a quadratic bivariate function f, whose quadratic form is indefinite and therefore has a hyperbolic paraboloid Φ as its graph surface. In case that the approximant is defined over a tessellation consisting of convex tiles and interpolating at the vertices, the tiles of an optimal solution are rhombic with isotropic diagonals in the pE metric induced by f. It is the diagonal net of a tiling with parallelograms whose edges lie on projections of rulings of Φ.

Note that the graph polyhedron of a solution is both inscribed and circumscribed to the hyperbolic paraboloid Φ.

5.3. Semidefinite type

In this case we only have to consider the normal form $f(\mathsf{x}) = x_1^2$, and the graph surface is a parabolic cylinder. The maximum error on an edge with vertices $\mathbf{a} = (a_1, a_2)$ and $\mathbf{b} = (b_1, b_2)$

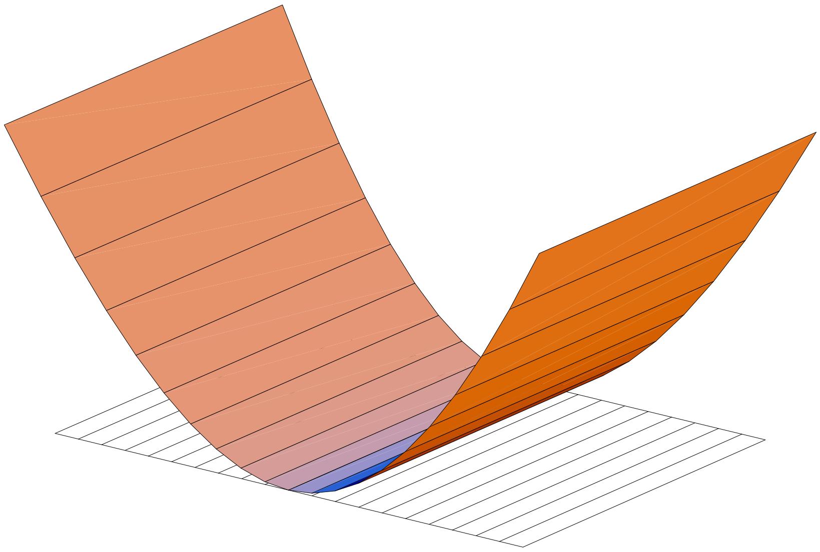

Figure 13: Optimal approximation in the semidefinite case

is

$$\epsilon = (b_1 - a_1)^2. \tag{21}$$

This reflects the obvious fact that the maximum error is not changed when projecting in x_2-direction.

Affine transformations characterized by equation (6) in $\mathbb{R}^2$, which do not change the maximum error, belong to the class of matrices A satisfying

$$A^t \cdot \begin{pmatrix} 1 & 0 \\ 0 & 0 \end{pmatrix} \cdot A = \begin{pmatrix} 1 & 0 \\ 0 & 0 \end{pmatrix}.$$

This implies

$$A = \begin{pmatrix} \pm 1 & 0 \\ a_{21} & a_{22} \end{pmatrix}. \tag{22}$$

The corresponding affine maps are called *length-preserving similarities* in the *isotropic plane* (sometimes called *Galilean plane* [37]). The error defined by equation (21) is the square of the isotropic distance of the two points **ab**. It vanishes for so-called isotropic lines (projections of the rulings of Φ). The L^p error is preserved if we additionally require $\det A = \pm 1$, i.e., $a_{22} = \pm 1$. These transformations contain the group of so-called *isotropic motions*,

$$\begin{aligned} x'_1 &= a + x_1, \\ x'_2 &= b + cx_1 + x_2. \end{aligned} \tag{23}$$

Optimal piecewise linear approximants in the L^∞ sense stem from optimal piecewise linear approximants of the univariate function $f(x_1) = x_1^2$. For these, the knots must be placed equidistantly. For practical considerations, it is sufficient to define the linear functions of an approximant over parallel strips with equal width. The sides are parallel to the x_2 axis. Concerning the graph, we obtain an approximant of the parabolic cylinder Φ by a prismatic surface with edges parallel to the rulings of Φ. The maximum error occurs at the edges and the "midlines" of the faces (Figure 13).

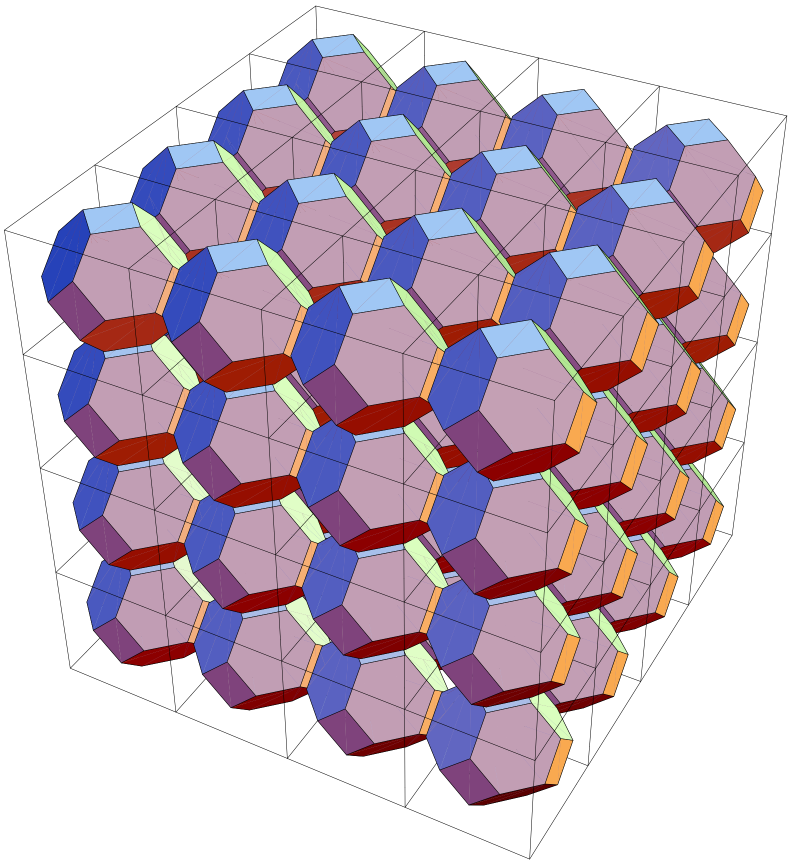

Figure 14: Cubo-octahedra as Voronoi cells of a body-centered cube grid

6. Trivariate functions

6.1. Definite type

We only have to consider the normal case $f(\mathbf{x}) = x_1^2 + x_2^2 + x_3^2$. The induced metric in $\mathbb{R}^3$ is the canonical Euclidean metric.

The problem of an optimal tessellation using tetrahedra is more complicated than for bivariate functions. It is well-known that among all tetrahedra with a given circumsphere the regular tetrahedron has the largest volume. However, congruent regular tetrahedra do not tile $\mathbb{R}^3$, nor do general congruent tetrahedra tile $\mathbb{R}^3$. An adapted concept of optimality for optimal tessellations with tetrahedra will be a subject of future research.

Let us now move to lattice tilings. There are five types of Voronoi cells that may occur (see the figure on page 917 of Volume B of [23]): parallelotope, hexagonal prism, rhombic dodecahedron, elongated dodecahedron, and cubo-octahedron (also called truncated octahedron). Prescribing the volume of the tiles, we conjecture that the smallest diameter is obtained in a special situation of the latter case: the underlying lattice is a cube grid plus the midpoints of the cubes. It is called *body-centered cube lattice*. The corresponding Voronoi cell is a cubo-octahedron (see Figure 14); it possesses a circumsphere [9].

The only result from convexity which solves an instance of the problems being discussed is deduced from the solution of the moment problem in $\mathbb{R}^3$ by Barnes and Sloane [3], which refers to the case $\omega(t) = t^2$, i.e., to the L^1 error when we assume a circumscribed graph polytope. The optimal lattice for this case is the body-centered cube lattice.

6.2. Indefinite type and semidefinite types

It is rather complicated to answer the indefinite case, where the normal form is $f(\mathbf{x}) = x_1^2 + x_2^2 - x_3^2$. The semidefinite cases reduce to lower dimensional situations and thus do not require a special treatment. For example, $f(\mathbf{x}) = x_1^2 + x_2^2$ viewed as a trivariate function yields hexagonal prismatic tessellations over a regular hexagonal tiling in the x_1x_2-plane.

Conclusion and future research

We have discussed optimal piecewise linear approximation of quadratic functions. It turned out that a variety of results from convex and discrete geometry is available for the bivariate, definite case. We could also settle the indefinite case in two dimensions, if we use the L^∞ error; studying the L^p error is a topic for future research.

From the practical point of view, the results in two dimensions give us sufficient information on the behavior of optimal approximants of bivariate quadratic functions.

An important topic for future research is the application of this knowledge to the construction of piecewise linear approximants of bivariate functions with nearly optimal knot placement. For example, a local quadratic approximation provides information on the local behavior of an optimal piecewise linear approximation. One way to apply this, is in form of criteria for mesh decimation algorithms. Moreover, it seems realistic to construct nearly optimal approximants via local quadratic fits and appropriate merging of the local solutions. A theoretical foundation for this approach in case of positive curvature has recently been provided by P.M. Gruber [24]. It should be pointed out that everywhere locally optimal approximants do not exist in general; asymptotically this would be possible only if the Riemannian or pseudo-Riemannian metric induced on the graph surface by its second fundamental form is flat.

In higher dimensions, the problem is much harder. However, it should be possible to solve the L^∞ case for $n = 3$ and thereby provide a basis for knot placement algorithms in piecewise linear approximants to trivariate functions.

Data reduction and hierarchical approximation schemes are extremely important in the context of analyzing and visualizing the massive data sets resulting from either numerical simulations of physical phenomena or high-resolution imaging. The methods we have presented in this paper have great promise to impact future research supporting reduction and hierarchical approximation in this context.

Acknowledgements

We are obliged to Professor P.M. Gruber and Dr. M. Ludwig for their advice and pointers to the literature.

The last three authors were supported by the National Science Foundation under contract ACI 9624034 (CAREER Award), the Office of Naval Research under contract N00014-97-1-0222, the Army Research Office under contract ARO 36598-MA-RIP, the NASA Ames Research Center through an NRA award under contract NAG2-1216, the Lawrence Livermore National Laboratory through an ASCI ASAP Level-2 under contract W-7405-ENG-48 (and B335358, B347878), and the North Atlantic Treaty Organization (NATO) under contract CRG.971628 awarded to the University of California, Davis. We also acknowledge the support of Silicon Graphics, Inc., and thank the members of the Visualization Thrust at the Center for Image Processing and Integrated Computing (CIPIC) at the University of California, Davis.

References

[1] P.K. Agarwal, P.K. Desikan: *An efficient algorithm for terrain simplification.* Proc. 8th ACM/SIGACT-SIAM Symposium on Discrete Algorithms (SODA '97), Association for Computing Machinery, New York 1997, 139–147.

[2] F. Aurenhammer: *Power diagrams: properties, algorithms and applications.* SIAM J. Computing **16**, 78–96 (1987).

[3] E.S. Barnes, N.J.A. Sloane: *The optimal lattice quantizer in three dimensions.* SIAM J. Algebraic Discrete Methods **4**, 30-41 (1983).

[4] W. Benz: *Geometrische Transformationen.* Bibliograph. Institut, Mannheim 1992.

[5] A. Beutelspacher, B. Petri: *Der goldene Schnitt.* Bibliograph. Institut, Mannheim 1988.

[6] G.P. Bonneau, S. Hahmann, G.M. Nielson: *BLaC-wavelets: A multiresolution analysis with non-nested spaces.* In: R. Yagel, G.M. Nielson (eds.): *Visualization '96*, IEEE Computer Society Press, Los Alamitos, CA, 1996, 43–48.

[7] K. Böröczky Jr., M. Ludwig: *Approximation of convex bodies and a momentum lemma for power diagrams.* Monatsh. Math. **127**, 101–110 (1999).

[8] P. Cignoni, L. De Floriani, C. Montani, E. Puppo, R. Scopigno: *Multiresolution modeling and visualization of volume data based on simplicial complexes.* In: A.E. Kaufman, W. Krüger (eds.): *1994 Symposium on Volume Visualization*, IEEE Computer Society Press, Los Alamitos, CA, 1994, 19–26.

[9] H.S.M. Coxeter: *Regular Polytopes.* Dover Publications, Inc., New York 1973.

[10] P. Desnoguès, O. Devillers: *A locally optimal triangulation of the hyperbolic paraboloid.* Proc. 7th Canad. Conf. Comp. Geom. 1995, 49–54.

[11] N. Dyn, D. Levin, S. Rippa: *Data dependent triangulations for piecewise linear interpolation.* IMA J. Numerical Analysis **10**, 137–154 (1988).

[12] N. Dyn, D. Levin, S. Rippa: *Algorithms for the construction of data dependent triangulations.* In: J.C. Mason, M.G. Cox (eds.): *Algorithms for Approximation II*, Chapman and Hall, New York 1990, 185–192.

[13] M. Eck, A.D. DeRose, T. Duchamp, H. Hoppe, M. Lounsbery, W. Stuetzle: *Multiresolution analysis of arbitrary meshes.* In: R. Cook (ed.): *Proceedings of SIGGRAPH 1995*, ACM Press, New York 1995, 173–182.

[14] H. Edelsbrunner: *Algorithms in Combinatorial Geometry.* Springer, 1987.

[15] L. Fejes Tóth: *Lagerungen in der Ebene, auf der Kugel und im Raum.* 2nd ed., Springer, Berlin 1972.

[16] T.S. Gieng, B. Hamann, K.I. Joy, G.L. Schussman, I.J. Trotts: *Constructing hierarchies for triangle meshes.* IEEE Transactions on Visualization and Computer Graphics **4**, 145–161 (1998).

[17] O. Giering: *Vorlesungen über höhere Geometrie.* Vieweg, Braunschweig - Wiesbaden 1982.

[18] M.H. Gross, R. Gatti, O. Staadt: *Fast multiresolution surface meshing.* In: G.M. Nielson, D. Silver (eds.): *Visualization '95*, IEEE Computer Society Press, Los Alamitos, CA, 1995, 135–142.

[19] R. Grosso, C. Lürig, T. Ertl: *The multilevel finite element method for adaptive mesh optimization and visualization of volume data.* In: R. Yagel, H. Hagen (eds.): *Visualization '97*, IEEE Computer Society Press, Los Alamitos, CA, 1997, 387–394.

[20] P.M. Gruber: *Volume approximation of convex bodies by inscribed polytopes.* Math. Ann. **281**, 229–245 (1988).

[21] P.M. Gruber: *Volume approximation of convex bodies by circumscribed polytopes.* The Victor Klee Festschrift, DIMACS Ser **4**, Americ. Math. Soc., Providence, RI, 1991, 309–317.

[22] P.M. Gruber: *Asymptotic estimates for best and stepwise approximation of convex bodies II.* Forum Math. **5**, 521–538 (1993).

[23] P.M. Gruber, J.M. Wills eds.: *Handbook of Convex Geometry.* Volumes A and B, North Holland, Amsterdam 1993.

[24] P.M. Gruber: *Optimal arrangement of finite point sets in Riemannian 2-manifolds.* Proc. Steklov Math. Inst. (1999), to appear.

[25] B. Hamann: *A data reduction scheme for triangulated surfaces.* Comput. Aided Geom. Des. **11**, 197–214 (1994).

[26] B. Hamann: *Curvature approximation of 3D manifolds in 4D space.* Comput. Aided Geom. Des. **11**, 621–633 (1994).

[27] B. Hamann: *Curvature approximation for triangulated surfaces.* In: G. Farin, H. Hagen, H. Noltemeier (eds.): *Geometric Modeling*, Computing Suppl. 8, Springer 1993, 139–153.

[28] B. Hamann, B.W. Jordan, D.A. Wiley: *On a construction of a hierarchy of best linear spline approximations using repeated bisection.* IEEE Transactions on Visualization and Computer Graphics **5** (1999).

[29] H. Hoppe: *Progressive meshes.* In: H. Rushmeier (ed.): *Proceedings of SIGGRAPH 1996*, ACM Press, New York 1996, 99–108.

[30] J. Hoschek, D. Lasser: *Fundamentals of Computer Aided Geometric Design.* A.K. Peters, Wellesley, MA, 1993.

[31] H.E. Huntley: *The Divine Proportion — A Study in Mathematical Beauty.* Dover Publ., New York 1970.

[32] E. Melissaratos: *L^p-optimal d-dimensional triangulations for piecewise linear interpolation: a new result on data dependent triangulations.* Technical Report CS-93-13, Dept. of Computer Science, Utrecht University, 1993.

[33] E. Nadler: *Piecewise linear best L^2 approximation on triangulations.* In: C.K. Chui, L.L. Schumaker, J.D. Ward (eds.): *Appoximation Theory*, Academic Press, Boston 1986, 499–502.

[34] G.M. Nielson, I.-H. Jung, J. Sung: *Haar wavelets over triangular domains with applications to multiresolution models for flow over a sphere.* In: R. Yagel, H. Hagen (eds.): *Visualization '97*, IEEE Computer Society Press, Los Alamitos, CA, 1997, 143–149.

[35] H. Pottmann, M. Peternell: *Applications of Laguerre geometry in CAGD.* Comput. Aided Geom. Des. **15**, 165–186 (1998).

[36] I.J. Trotts, B. Hamann, K.I. Joy, D.F. Wiley: *Efficient and robust simplification of tetrahedral meshes.* In: D.S. Ebert, H. Hagen, H.E. Rushmeier (eds.): *Visualization '98*, IEEE Computer Society Press, Los Alamitos, CA, 1998, 287–295.

[37] I.M. Yaglom: *A Simple Non-Euclidean Geometry and its Physical Basis.* Springer, New York - Heidelberg - Berlin 1979.

[38] J.C. Xia, A. Varshney: *Dynamic view-dependent simplification for polygonal meshes.* In: R. Yagel, G.M. Nielson (eds.): *Visualization '96*, IEEE Computer Society Press, Los Alamitos, CA, 1996, 327–334.

Received January 12, 2000